Excited-state enhancement of third-order nonlinear optical responses in conjugated organic chains

D.C. Rodenberger, J.R. Heflin,* and A.F. Garito
Department of Physics, University of Pennsylvania, 209 South 33rd Street, Philadelphia, Pennsylvania 19104
(Received 8 June 1993; revised manuscript received 11 April 1994)

We present the details of an experimental observation of excited-state enhancement of the degenerate-four-wave-mixing (DFWM) susceptibility $\gamma^{S_n}(-\omega;\omega,\omega,-\omega)$ of a conjugated linear chain, diphenylexatriene (DPH), when the first π-electron excited state is populated for nanosecond time scales and then probed nonresonantly through picosecond DFWM. An increase as large as a factor of 100 in the completely nonresonant 1064-nm DFWM signal from the highest DPH concentrations (8 mM) is observed when the 355-nm pump beam saturates the S_2 absorption as compared to when the pump beam is turned off. A large $\gamma^{S_2}(-\omega;\omega,\omega,-\omega)$ of $(12\,000 \pm 1700) \times 10^{-36}$ esu is found, compared to the ground state $\gamma^{S_0}(-\omega;\omega,\omega,-\omega)$ which is $< 50 \times 10^{-36}$ esu. Importantly, separate transient absorption experiments show that there is no excited-state absorption at 1064 nm with excitation at 355 nm. Therefore, upon population of the excited state, the electronic third-order optical susceptibility of DPH is increased by orders of magnitude, without introducing any optical loss at the probe wavelength.

PACS number(s): 42.50.−p, 78.47.+p, 42.65.−k

I. INTRODUCTION

Conjugated organic molecules and polymer systems are of interest due to the delocalized π-electron systems which give rise to large values of $\chi^{(3)}$, with extremely fast response times, in wavelength regimes where there is minimal background absorption [1–5]. We have previously presented theoretical results demonstrating that $\chi^{(3)}$ can be further increased for nonlinear optical processes originating from a real population of electronic excited states in conjugated linear chains [6]. Compared with the ground state, the calculated nonresonant third-order optical susceptibility $\chi^{(3)}(-\omega_4;\omega_1,\omega_2,\omega_3)$ of π-conjugated linear-chain molecules can be enhanced by orders of magnitude, and even change sign, when the first (S_1) or second (S_2) electronic excited state is optically pumped and then populated for times long enough to perform nonresonant measurements of $\chi^{(3)}(-\omega_4;\omega_1,\omega_2,\omega_3)$ at frequencies different from the resonant pump frequency.

Importantly, the excited-state enhanced nonlinear optical response is observed for wavelengths that are nonresonant for both ground- and excited-state populations. A nonlinear optical process is said to be nonresonant when the wavelengths involved are away from any absorbing electronic transitions. Resonant processes generally have much larger nonlinear susceptibilities, but are slower because real electronic excitations occur; they also involve considerable absorptive loss of the optical beam. Nonresonant processes, as they involve only virtual electronic excitations, are essentially instantaneous, and avoid attenuation of the optical signal.

The third-order nonlinear optical susceptibility is denoted $\chi^{(3)}(-\omega_4;\omega_1,\omega_2,\omega_3)$, where $\omega_4 = \omega_1+\omega_2+\omega_3$ is the frequency of the output light in response to light input at frequencies ω_1, ω_2, and ω_3. One standard method for measurement of $\chi^{(3)}(-\omega;\omega,\omega,-\omega)$, corresponding to the intensity dependent index of refraction n_2, is degenerate-four-wave mixing (DFWM) in which two optical beams form a phase or intensity grating that modulates the refractive index of a material and a third beam scatters from the grating into a new direction. In this paper we describe enhancement of the DFWM susceptibility $\chi^{(3)}(-\omega;\omega,\omega,-\omega)$ of a linear conjugated molecule, diphenylhexatriene (DPH), when the first one-photon allowed π-electron excited state is populated for nanoseconds and then probed nonresonantly through picosecond DFWM.

Saturably absorbing systems can be used to study the dependence of the nonlinear optical susceptibility on excited states. When optically pumped, such an absorber can maintain a large excited-state population for times long enough to carry out nonlinear optical measurements on the excited state. The first experimental observation of enhanced nonlinear optical response by excited state population was made by third-harmonic-generation (THG) measurements of the conjugated disklike structure, silicon naphthalocyanine (SINC) [7]. When solutions of SINC were optically pumped at 770 nm in the strong Q-absorption band to populate the first electronic excited state (S_1), and then probed by 30-ps pulses at 1543 nm, the THG Maker fringe amplitude was seen to decrease significantly because of a very large and negative $\gamma^{S_1}(-3\omega;\omega,\omega,\omega)$ of $(1640 \pm 100) \times 10^{-36}$ esu from the S_1 excited state of SINC that is orders of magnitude larger than the ground state $|\gamma^{S_0}(-3\omega;\omega,\omega,\omega)|$ which is $< 10 \times 10^{-36}$ esu. A small excited-state absorption is also observed in SINC, however, so that the enhancement created by the excited-state population is accompanied by absorption of the probe wavelength.

In this paper, the active nonlinear optical material is DPH (Fig. 1), which exhibits saturable absorption from the S_0 ($1\,^1A_g$) ground state to the S_2 ($1\,^1B_u$) excited state centered near 355 nm, an excited-state lifetime of

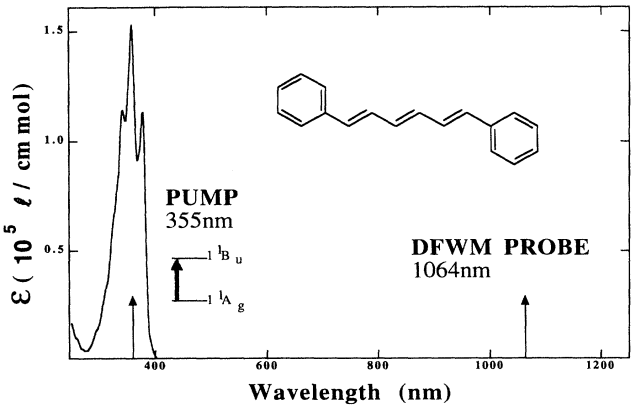

FIG. 1. Diphenylhexatriene (DPH) absorption spectrum and molecular structure. One absorption band occurs near 355 nm for the $S_0 \rightarrow S_2$ transition. The π-conjugated bonds of DPH create large nonresonant nonlinear optical responses. In this experiment, the pump excites the 355-nm absorption while the DFWM probe occurs off-resonance at 1064 nm.

several nanoseconds, and transparency for wavelengths from 400 nm to greater than 2000 nm [8,9]. Excitation to the S_2 state is known to lead additionally to population of the S_1 ($2\,^1A_g$) state, which lies at a slightly lower energy [10]. The strict parities observed for the electronic states demonstrate that DPH is centrosymmetric in both the ground and excited states [20]. Accordingly, there is a negligible fraction of the noncentrosymmetric *cis*-isomer. We have separately observed that DPH exhibits no excited-state absorption at 1064 nm with excitation at 355 nm, so that the excited-state nonlinear optical properties observed are not affected by potential changes in the absorption upon population of the excited state.

The DFWM experiment is carried out using two orthogonally polarized, 1064-nm probe beams and a 355-nm pump beam. Coherent interaction of the two probes in the sample produces diffraction of each probe from a grating written in the sample, proportional to the square of the third-order nonlinear optical susceptibility $\chi^{(3)}(-\omega;\omega,\omega,-\omega)$. The unique feature of our experimental configuration is the introduction of an intense optical pump beam tuned to the first electronic absorption band of the material which causes a large fraction of the molecules in the sample to occupy the first optical excited state. An increase as large as a factor of 100 in the completely nonresonant 1064-nm DFWM signal from the highest DPH concentrations is observed when the 355-nm pump beam saturates the S_2 absorption as compared to when the pump beam is turned off. Calculations [6] have shown that any possible orientational contributions to $\chi^{(3)}(-\omega;\omega,\omega,-\omega)$ due to the small ground- and excited-state linear polarizabilities are much smaller than the corresponding electronic contributions. The observed enhancement is, therefore, a result of an increase in the molecular electronic contribution to $\chi^{(3)}(-\omega;\omega,\omega,-\omega)$ by orders of magnitude.

II. THEORY

A. Excited-state nonlinear optics

In studies recently published, we used calculations of the electronic molecular third-order nonlinear optical susceptibility to predict a general enhancement that occurs when a molecule resides in an excited state, rather than in the ground state [6]. In these theoretical studies of microscopic third-order optical susceptibilities $\gamma_{ijkl}(-\omega_4;\omega_1,\omega_2,\omega_3)$ of quasi-one-dimensional (1D) and quasi-two-dimensional (2D) chainlike and disklike conjugated organic structures, we found that compared to the ground-state nonresonant $\gamma_{ijkl}(-\omega_4;\omega_1,\omega_2,\omega_3)$ [11,12], the susceptibility can markedly increase in magnitude and even change sign, when the π-electron excited state is populated. The principal reasons for the enhancement are the larger optical transition moments $\mu_{nn'}$ and smaller excitation energies $\hbar\omega_{nn'}$ between excited states S_n and $S_{n'}$, especially for highly charge correlated virtual excitations, and a reduced degree of competition between virtual excitation processes that contribute with opposite signs to determine the magnitude, sign, and dispersion of $\gamma_{ijkl}(-\omega_4;\omega_1,\omega_2,\omega_3)$. The electron-correlation microscopic origin of the ground state $\gamma_{ijkl}(-\omega_4;\omega_1,\omega_2,\omega_3)$ has been experimentally confirmed through a series of dc-induced second-harmonic-generation and third-harmonic-generation dispersion measurements of key conjugated linear-chain structures [13].

B. Excited-state population: two level approximation

Many saturable absorber systems, including DPH, can be treated in the two level system approximation. When a monochromatic pump field is tuned to the resonant frequency, the rate equations for the populations of the ground and excited states can be written [14],

$$\frac{\partial \rho_e}{\partial t} = -R(\rho_e - \rho_g) - \frac{\rho_e}{T_1}, \tag{2.1}$$

$$\frac{\partial \rho_g}{\partial t} = +R(\rho_e - \rho_g) + \frac{\rho_e}{T_1}, \tag{2.2}$$

where ρ_g and ρ_e are the diagonal elements of the density matrix corresponding to the fractional populations of the ground and excited states, respectively ($\rho_g+\rho_e = 1$). The steady-state solution to these equations is

$$\rho_g = \frac{1}{2}\left[1 + \frac{I_S}{I + I_S}\right], \tag{2.3}$$

$$\rho_e = \frac{1}{2}\left[1 - \frac{I_S}{I + I_S}\right], \tag{2.4}$$

where

$$I_S = \frac{\hbar\omega}{2\sigma T_1}, \tag{2.5}$$

σ is the absorption coefficient, and T_1 is the excited-state lifetime [15]. Saturation of such an absorbing system

is characterized by equal population of the excited and ground states, and zero background absorption. In a separate publication [16], we will describe in more detail the dynamics among the S_0, S_1, and S_2 states of DPH and the contributions of each to the time dependence of the excited state $\chi^{(3)}$.

DPH is a conjugated linear-chain molecule whose linear optical properties have been well studied [8–10,17–21]. It has a strongly peaked absorption band near 350 nm, above which it is essentially transparent, with no absorptions from 400 nm to over 2000 nm (Fig. 1). Relaxation from the excited state occurs principally through fluorescence from 350 nm to 500 nm with a lifetime of order 1 ns to 15 ns depending on solvent polarizability. The present study was performed using dilute (1–8 mM) solutions of DPH in anhydrous dioxane which exhibit lifetimes in the range of 2 ns to 8 ns, depending on concentration.

We can understand the absorption and fluorescence characteristics of DPH by considering the electronic-state ordering diagram in Fig. 2. The absorption band is represented by a transition from the S_0 ($1\,^1A_g$) state to the S_2 ($1\,^1B_u$) excited state. A 355-nm pump from the third harmonic of a Nd:YAG (yttrium aluminum garnet) laser populates only the $1\,^1B_u$ excited-state manifold since one-photon transitions from the $1\,^1A_g$ ground state to the S_1 ($2\,^1A_g$) excited state are forbidden. High-resolution absorption and fluorescence studies have established the location of this lower-lying $2\,^1A_g$ state [18]. The location of the S_2 state depends on temperature and solvent polarizability [9,18]. Depopulation of the S_2 state occurs by internal conversion to the S_1 ($2\,^1A_g$) state, and since the energy gap ΔE between S_1 and S_2 is small (of order 215 cm^{-1}), thermal equilibrium is established between the two states. At room temperature, equilibrium occurs approximately 50 ps after excitation [10,18]. The populations of the S_1 and S_2 states decay together to the ground state by fluorescence and by nonradiative decay, with a fluorescence quantum yield of 0.64 at room temperature [9] and a lifetime of 7.8 ns in dioxane. The fluorescence lifetime is larger (up to 15 ns in methylpentane) for nonpolar solvents and smaller (as low as 0.7 ns in ethyliodide) in strongly polar solvents. Solvent polarity also effects the fluorescence quantum yield, which approaches unity in nonpolar solvents at low temperatures.

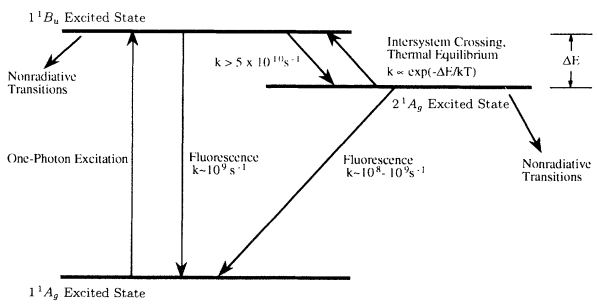

FIG. 2. Electronic states energy diagram of DPH. Excitation at 355 nm causes absorption from $S_0(1\,^1A_g)$ to the $S_2(1\,^1B_u)$ excited state. Rapid intersystem crossing populates the $S_1(2\,^1A_g)$ state, and because the energy gap ΔE between S_1 and S_2 is small, on the order of 215 cm^{-1}, a thermal equilibrium is established within 50 ps in the population of the two states. The populations decay with a lifetime of 7.8 ns (in dilute solutions of dioxane).

For the purposes of this study of the excited-state enhancement of the nonlinear optical response, the precise identification of the excited-state population is not critical. We, therefore, will speak of the excited-state enhancement to be the result of the S_2 state alone so as not to complicate the discussion of the excited-state nonlinearity. Once the relative populations of the S_1 and S_2 states are known as a function of time after the excitation, we may separate the nonlinear response into a sum of contributions from the S_1 and S_2 states [16].

C. Excited-state nonresonant nonlinear optics

The third-order nonlinear optical susceptibility $\chi^{(3)}$ depends on the state occupation of the molecules in the material. The macroscopic susceptibility for any set of electronic states can be expressed as

$$\chi^{(3)} = FN \sum_n \rho_n \gamma^n, \tag{2.6}$$

where F is the local field factor, N is the number density, and γ^n is the molecular susceptibility for the state n of the nonlinear optical molecule.

In a solution, the combined macroscopic susceptibility includes contributions from the solvent and the solute molecules. If we assume the solvent undergoes no population change due to excitation of the saturable absorber solute molecules, then we may write

$$\chi^{(3)} = FN_1\gamma^{\text{solvent}} + FN_2[\rho_g\gamma^g + \rho_e\gamma^e], \tag{2.7}$$

where N_1 and N_2 are the number densities of the solvent and solute molecules, respectively. We may utilize the linear nature of this relation to derive the values of γ^{solvent}, γ^g, and γ^e from experimental observations of $\chi^{(3)}$. Upon saturation of the absorber system, the population densities become $\rho_g = \rho_e = \frac{1}{2}$. The susceptibility $\chi^{(3)}$ then depends linearly on $(\gamma^g + \gamma^e)$ and concentration so that $\gamma^e + \gamma^g$ is determined by a study of $\chi^{(3)}$ versus concentration,

$$\chi^{(3)} = F[N_1\gamma^{\text{solvent}} + N_A c(\rho_g\gamma^g + \rho_e\gamma^e)], \tag{2.8}$$

where F is a local field factor, c is in units of moles/cm^3, and the coefficient of $\chi^{(3)}$ depending on c is

$$\frac{\partial\chi^{(3)}}{\partial c} = FN_A(\rho_g\gamma^g + \rho_e\gamma^e). \tag{2.9}$$

Without resonant excitation of the saturable absorber system, $\chi^{(3)}$ depends linearly on γ^g and concentration so that

$$\chi^{(3)} = F[N_1\gamma^{\text{solvent}} + N_A c\rho_g\gamma^g], \tag{2.10}$$

and the coefficient of $\chi^{(3)}$ depending on c is

$$\frac{\partial\chi^{(3)}}{\partial c} = FN_A\rho_g\gamma^g. \tag{2.11}$$

III. EXPERIMENT

We measure the third-order nonlinear optical susceptibility $\chi^{(3)}_{ijkl}(-\omega;\omega,\omega,-\omega)$, using DFWM in the forward phase conjugate geometry [22–26]. In this technique two probe beams of comparable intensity intersect in a thin sample of path length L, at a small angle to minimize the phase mismatch of the nonlinear process. The two optical beams form a phase grating that modulates the refractive index of the sample material, and a fraction of each beam scatters from the grating in a new direction. If the propagation vectors of the two probes are given by $\mathbf{k}_1$ and $\mathbf{k}_2$, then DFWM output beams are produced in the directions given by $2\mathbf{k}_2 - \mathbf{k}_1$ and $2\mathbf{k}_1 - \mathbf{k}_2$, and the signal intensity is proportional to the square of the third-order nonlinear optical susceptibility $\chi^{(3)}_{ijkl}(-\omega;\omega,\omega,-\omega)$. We choose the polarizations of the $\mathbf{k}_1$ and $\mathbf{k}_2$ probe beams to be orthogonal to eliminate thermal and population grating contributions from the DFWM signal. Specifically, $\mathbf{k}_1$ is horizontally polarized, $\mathbf{k}_2$ is vertically polarized, and we observe the horizontally analyzed signal in the $2\mathbf{k}_2 - \mathbf{k}_1$ direction, proportional to $|\chi^{(3)}_{xyyx}(-\omega;\omega,\omega,-\omega)|^2$. The unique feature of this experiment is that before the nonlinear probe occurs, the sample is first optically pumped to an electronic excited state. For probe delay times less than the nanosecond relaxation time of the excited state, the nonlinear probe encounters an excited-state population, and is, therefore, sensitive to the nonlinear optical susceptibility of the electronic excited state [27].

The excited state DFWM experiment begins with the arrival of a 30-ps pump beam resonant to the S_0 to S_2 absorption which excites the DPH to saturate the absorption, creating a population density $\rho_e = \frac{1}{2}$ in the S_2 excited state. After excitation, and before relaxation to the ground state occurs, the two DFWM probe pulses arrive, producing a diffracted signal with an intensity proportional to $|\chi^{(3)}_{xyyx}(-\omega;\omega,\omega,-\omega)|^2$. By controlling the intensity and timing of the pump beam with respect to the DFWM probe beams, the excited-state nonlinear optical susceptibility is compared with the ground-state susceptibility and is found to be greatly enhanced by the presence of the pump beam.

A. Apparatus

The excited-state forward phase conjugate DFWM experiment is shown in Fig. 3. Two 1064-nm probe beams are focused in coincidence on the sample at a small angle θ. The DFWM signal in the $2\mathbf{k}_2 - \mathbf{k}_1$ direction is detected by a photomultiplier tube (PMT). The angle θ in this experiment is determined by acceptable phase mismatch as a function of the sample path length and the wavelength by $\theta < \sqrt{\lambda/2L}$. With the angle θ fixed at 2.5 degrees, we use a 0.2-mm path length cell which satisfies the phase match criteria.

The 30-ps, 1064-nm pulses from an actively and passively mode-locked Nd:YAG laser are first doubled and then mixed in KD*P crystals to produce third-harmonic pulses at 355 nm. As shown in Fig. 4, the remaining 1064-nm beam is split into two equally intense beams, of approximately 1 mJ per pulse, which serve as the DFWM probes, each of which passes through a halfwave plate and a prism polarizer that allow selection of each polarization and intensity. The $\mathbf{k}_1$ beam polarization is selected to be horizontal (x) and the $\mathbf{k}_2$ beam polarization is selected to be vertical (y) for all of the DFWM experiment results described. The two beams travel along separately adjustable length arms and are focused to a 100-μm beam waist by a single lens onto the 0.2-mm path length fused silica sample flow cell containing the liquid DPH in dioxane samples. The DFWM signal output along the $2\mathbf{k}_2 - \mathbf{k}_1$ direction is isolated by a series of apertures and beam blocks, and brought through neutral density and interference wavelength filters into an IR sensitive (Varian model VPM-159A.120) PMT. At the same time, the 355-nm beam from the laser is delayed by an adjustable length path, passed through a halfwave plate and polarizer for control of polarization and intensity, and focused on the interaction region in the sample cell. Signals from the PMT are amplified using an emitter follower preamplifier, and sent to a gated integrator along

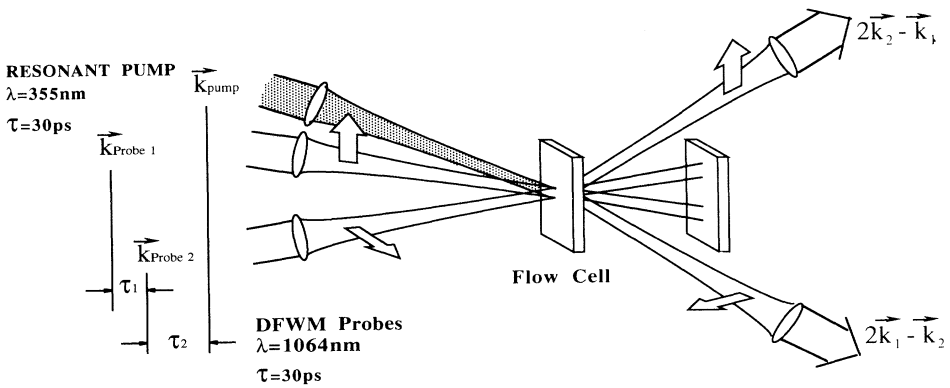

FIG. 3. Forward excited-state DFWM experiment. The $\mathbf{k}_1$ probe is horizontally polarized, the $\mathbf{k}_2$ probe is vertically polarized, and the approximately phase matched signal in the $2\mathbf{k}_2$-$\mathbf{k}_1$ direction is detected by a photomultiplier tube following a system of apertures and a horizontally oriented analyzing polarizer.

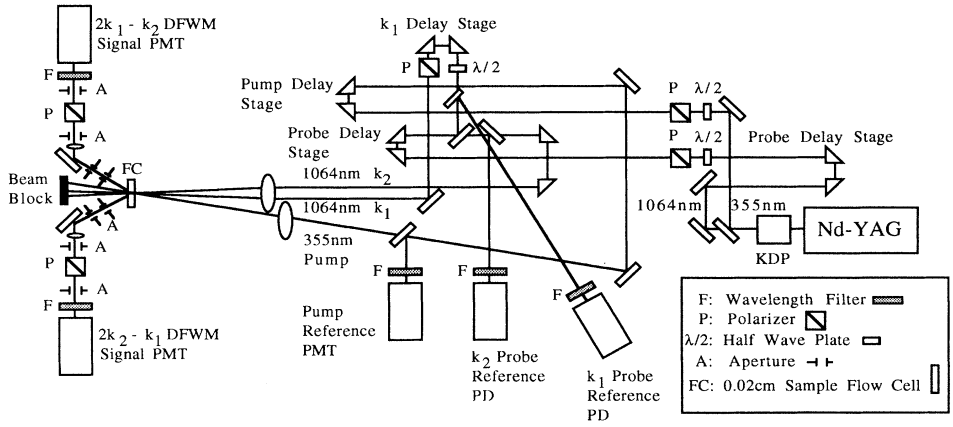

FIG. 4. Excited-state DFWM experiment layout. The 30-ps, 1064-nm beam is split into two equally intense beams that travel along separately adjustable length arms of a modified Michaelson interferometer where polarization and intensity may be selected. The DFWM signal output along the $2\mathbf{k}_2 - \mathbf{k}_1$ direction is isolated by a series of apertures and beam blocks, and brought through neutral density and interference wavelength filters and an analyzer into an IR sensitive (Varian model VPM-159A.120) PMT. Similarly, the 30-ps, 355-nm beam is appropriately delayed by an adjustable length path, and focused on the interaction region in the sample cell to create the excited-state population. PD denotes a photodiode and KDP is a potassium dihydrogen phosphate crystal.

with an appropriately delayed gate signal derived from a photodiode monitoring the laser pulses. A microcomputer controls the integrator using a CAMAC (computer automated measurement and control) interface, and accumulates statistics of the DFWM signal on a shot to shot basis. A computer controlled shutter system allows the computer to separately block each beam, in order to measure and subtract the linear scattering background. During each shot recorded by the computer, reference detectors are used to determine the intensities of the two probes and the pump beam for normalization of possible long term laser power drift. Computer control of the pump halfwave plate, probe arm delay translators, pump arm delay translator, and pump beam lens position allows the computer to quickly carry out measurements of the systematic dependences on pump intensity, relative probe delay, pump-probe delay, and pump-probe overlap, respectively. The intensities of the probes are recorded for reference comparisons between data points. Any drift in laser power levels can be compensated by appropriate normalization of the reference values. For example, the quantity

$$S = \frac{\mathrm{I_{DFWM}}}{I_{\mathbf{k}_1} I_{\mathbf{k}_2}^2} \tag{3.1}$$

is independent of laser fluctuation for the $2\mathbf{k}_2 - \mathbf{k}_1$ DFWM experiment, and the data are normalized on a shot to shot basis.

B. Experimental excited-state enhancement of DFWM

We observe enhancement in the completely nonresonant DFWM signal when the DPH samples are pumped into the S_2 excited state by a resonant pump. This enhancement is evident when we compare the DFWM autocorrelation of the probe pulses with and without excited-state enhancement (see Fig. 5). If the two probes arrive at different times, the DFWM signal depends on the autocorrelation function

$$A(t) = \int_{-\infty}^{\infty} U_1(t') U_2^2(t - t') dt, \tag{3.2}$$

where U_1 and U_2 are the amplitude envelope functions for the $\mathbf{k}_1$ and $\mathbf{k}_2$ probes. The autocorrelation is observed by changing the relative arrival times of the two probe pulses. At coincidence ($t = 0$), the DFWM signal is a maximum, and the signal decreases for increasing relative time delays ($|t| > 0$).

Enhancement produced by the pump is measured by comparing the amplitudes of the autocorrelation with the pump on and with the pump off. The relative arrival times of the $\mathbf{k}_1$ and $\mathbf{k}_2$ probe pulses are adjusted by an optical delay consisting of a corner reflector mounted on a translation stage aligned such that movement of the stage changes the path length but not the alignment of the reflected beam. The instantaneous nature of the DFWM signal can be seen by investigating the behavior of the

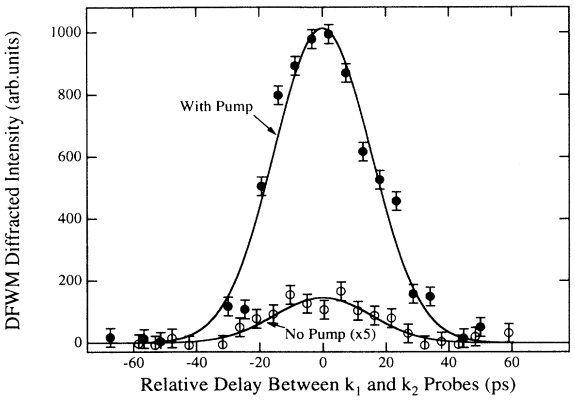

FIG. 5. Pump enhancement of the autocorrelation of the DFWM probes. Typical DFWM signal of DPH in dioxane with pump on and pump off as a function of time delay between the two probe beams. The pump delay is set such that the 355-nm, 30-ps pump pulse precedes the 30-ps, 1064-nm probes by 100 ps and the relative delay between the probe pulses is varied. The unpumped data, which has been multiplied by a factor of 5 for clarity, corresponds to the background signal from the dioxane solvent since the ground-state contribution from DPH is smaller than the detection resolution of the experiment. An enhancement of a factor of 37 in intensity is shown here for a concentration of 3×10^{-3} M.

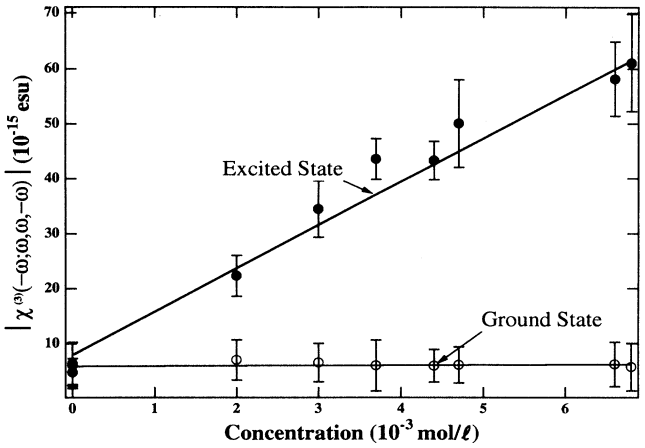

FIG. 6. The value of $\chi^{(3)}_{xyyx}(-\omega;\omega,\omega,\omega)$ as a function of concentration measured by DFWM in DPH solutions in dioxane. The upper line is a linear fit to the excited-state $\chi^{(3)}$ data, and its slope gives a value of $\gamma^{S_2}(-\omega;\omega,\omega,-\omega)$ of $(12\,000 \pm 700) \times 10^{-36}$ esu. The lower line is a linear fit to the ground-state $\chi^{(3)}$ data, and its zero slope gives an upper bound on the value of $|\gamma^{S_0}(-\omega;\omega,\omega,-\omega)| < 50 \times 10^{-36}$ esu. The ground state $\chi^{(3)}$ is, therefore, entirely due to the $\chi^{(3)}$ of the dioxane solvent alone.

signal with respect to the relative delay between the $\mathbf{k}_1$ and $\mathbf{k}_2$ probe pulses. With the pulse envelope functions modeled as Gaussian pulses, the autocorrelation is also a Gaussian with a width equal to $\sqrt{3/2}\tau_p$,

$$A(t) = e^{-(2t/3\tau_p)^2} \tag{3.3}$$

and centered about the zero relative delay position.

C. Quantitative characterization of the enhancement

The value of the microscopic third-order nonlinear optical susceptibility of DPH molecules in the ground and excited states can be determined through a study of the macroscopic $\chi^{(3)}(-\omega;\omega,\omega,-\omega)$ as a function of concentration. DPH can be dissolved in dioxane with concentrations up to nearly 10^{-2} M, and can produce an observable excited-state DFWM signal in concentrations down to 10^{-3} M. Within this range of concentrations, the signal amplitude, proportional to the third-order susceptibility squared $|\chi^{(3)}(-\omega;\omega,\omega,-\omega)|^2$, is observed for a series of samples. The data are compared on a plot of $\chi^{(3)}(-\omega;\omega,\omega,-\omega)$ versus concentration in Fig. 6. If the relation in Eq. (2.7) holds, we expect that the dependence of $\chi^{(3)}_{xyyx}(-\omega;\omega,\omega,-\omega)$ is linear with respect to concentration. The DFWM signal from the DPH liquid samples is referenced to a liquid sample of CS_2. The liquid samples can be interchanged without disturbing other experimental conditions, and we compute the signal intensity ratio,

$$\frac{I_{CS_2}}{I_{DPH}} = \frac{|\chi^{(3)}_{xyyx\,CS_2}|^2}{|\chi^{(3)}_{xyyx\,DPH}|^2} \tag{3.4}$$

which gives the value of the susceptibility with respect to the known value of

$$\chi^{(3)}_{xyyx\,CS_2}(-\omega;\omega,\omega,-\omega) = 3.6 \times 10^{-13} \text{ esu}, \tag{3.5}$$

for CS_2 given by Hellwarth [28]. Experimental comparison of the forward phase conjugate DFWM amplitude from CS_2 with that from dioxane alone yields

$$\chi^{(3)}_{xyyx\,\text{dioxane}} = (6.4 \pm 0.7) \times 10^{-15} \text{ esu} \tag{3.6}$$

as a reference value for the susceptibility of the host solvent for DPH, and will serve as the reference for this work.

When no pump beam is present, the ground-state molecular susceptibility of DPH $\gamma^{S_0}(-\omega;\omega,\omega,-\omega)$ and the dioxane solvent susceptibility $\gamma^{D}(-\omega;\omega,\omega,-\omega)$ contribute to the net observed macroscopic susceptibility according to Eq. (2.10),

$$\chi^{(3)}(-\omega;\omega,\omega,-\omega) = (f_\omega)^4[N_D\gamma_D(-\omega;\omega,\omega,-\omega) + cN_A\gamma^{S_0}(-\omega;\omega,\omega,-\omega)]. \tag{3.7}$$

where cN_A and N_D are the number densities of the ground-state DPH and dioxane molecules, respectively, and $f_\omega = \frac{n_\omega^2+2}{3}$ is the Lorentz-Lorenz local field factor. When the pump beam is present, however, the corre-

sponding macroscopic susceptibility from Eq. (2.8) is given by

$$\chi^{(3)}(-\omega;\omega,\omega,-\omega) = (f_\omega)^4[N_D\gamma_D(-\omega;\omega,\omega,-\omega) + c\rho_g N_A\gamma^{S_0}(-\omega;\omega,\omega,-\omega) + c\rho_e N_A\gamma^{S_2}(-\omega;\omega,\omega,-\omega)], \quad (3.8)$$

where $c\rho_e N_A$ and γ^{S_2} are the corresponding number densities of molecules and molecular susceptibility for the S_2 excited state of DPH. Since the solvent dioxane is transparent at 1064 nm and far from any electronic resonances, $\gamma_D(-\omega;\omega,\omega,-\omega)$ is positive and real. Here, we have assumed that γ^{S_0} and γ^{S_2} are also real. If there are any imaginary parts, they will appear as nonlinear terms in the expression for $\chi^{(3)}$ as a function of concentration. Since $\chi^{(3)}$ is observed to be linear within experimental uncertainties, we conclude that the imaginary part is zero.

As shown in Fig. 6, the measured values of $\chi^{(3)}_{xyyx}(-\omega;\omega,\omega,-\omega)$ are linearly dependent on the concentration of the solution, with a slope, from Eq. (3.8) of

$$\left.\frac{\partial\chi^{(3)}_{xyyx}(-\omega;\omega,\omega,-\omega)}{\partial c}\right|_{\text{with pump}} = [\rho_e N_A\gamma^{S_2}(-\omega;\omega,\omega,-\omega) + \rho_g N_A\gamma^{S_0}(-\omega;\omega,\omega,-\omega)] \quad (3.9)$$

when the pump beam is present, and a slope from Eq. (3.7) of

$$\left.\frac{\partial\chi^{(3)}_{xyyx}(-\omega;\omega,\omega,-\omega)}{\partial c}\right|_{\text{no pump}} = \rho_g N_A\gamma^{S_0}(-\omega;\omega,\omega,-\omega) \quad (3.10)$$

when no pump beam is present. The unpumped DFWM signal is observed to be independent of concentration, demonstrating that the ground state $\gamma^{S_0}(-\omega;\omega,\omega,-\omega)$ for DPH is smaller than the experimental resolution of $\pm 50 \times 10^{-36}$ esu, and thus the unpumped signal is due entirely to the dioxane solvent contribution in Eq. (3.7). The resolution is determined by the uncertainty in the slope of the linear fit to the ground-state $\chi^{(3)}_{xyyx}(-\omega;\omega,\omega,-\omega)$ data versus concentration. The pumped DFWM signal, however, increases strongly with increased DPH concentration, and the linear fit yields a value for $\gamma^{S_2}(-\omega;\omega,\omega,-\omega)$,

$$\gamma^{S_2}(-\omega;\omega,\omega,-\omega) = (12\,000 \pm 700) \times 10^{-36} \text{ esu} \quad (3.11)$$

showing that the excited state $\gamma^{S_2}(-\omega;\omega,\omega,-\omega)$ in Eq. (3.8) is more than two orders of magnitude larger than the ground state $\gamma^{S_0}(-\omega;\omega,\omega,-\omega)$.

The technique used to determine the magnitude of $\gamma^{S_2}(-\omega;\omega,\omega,-\omega)$ also determines the sign. Consider the case where γ^{S_2} is negative in sign. Since $\chi^{(3)}$ involves a sum of the solvent contribution ($\gamma_D > 0$) and the excited-state contribution from γ^{S_2}, then we expect for a critical value of the concentration, the two contributions will exactly cancel. The effect would be to observe, as a function of concentration, first a negative slope starting from the zero concentration $\chi^{(3)}$ value, followed by a minimum (or complete cancellation since γ^{S_2} has no imaginary part) and then a positive slope. If γ^{S_2} is positive in sign, no such cancellation occurs. Inspection of the data in Fig. 6 reveals that $\chi^{(3)}$ increases monotonically from zero concentration, and the sign of γ^{S_2} is positive.

D. Polarization and $\chi(3)$

The polarization of the probe beams and detector analyzer determines which of the different tensor components of the third-order nonlinear optical susceptibility produce the DFWM signal. In the $2\mathbf{k}_2 - \mathbf{k}_1$ forward phase conjugate DFWM experiment, the detected polarization follows the $\mathbf{k}_1$ probe polarization, and the experiment can be carried out in one of four polarization configurations: both probes horizontally polarized and detection horizontal ($xxxx$), both probes vertically polarized and detection vertical ($yyyy$), the $\mathbf{k}_1$ probe horizontal, the $\mathbf{k}_2$ probe vertical, and detection horizontal ($xyyx$), and the $\mathbf{k}_1$ probe vertical, the $\mathbf{k}_2$ probe horizontal, and detection vertical ($yxxy$). The tensor component subscripts enumerate the polarizations of the detected beam, both photons in the $\mathbf{k}_2$ probe, and the $\mathbf{k}_1$ probe, respectively (the $\mathbf{k}_2$ probe is indicated twice in the tensor component because it contributes two photons to the process). In an isotropic liquid, the $xxxx$ and $yyyy$ configurations both measure the $\chi^{(3)}_{xxxx}(-\omega;\omega,\omega,-\omega)$ component of the susceptibility, which includes such effects as thermal and density gratings unrelated to the electronic nonlinear optical susceptibility. The $xyyx$ and $yxxy$ configurations both measure the $\chi^{(3)}_{xyyx}(-\omega;\omega,\omega,-\omega)$ component of the susceptibility, which depends only on the electronic and orientational contributions to the susceptibility. We, therefore, use the $xyyx$ configuration to measure the excited-state dependence of the electronic nonlinear optical susceptibility $\chi^{(3)}_{xyyx}(-\omega;\omega,\omega,-\omega)$, employing an interference filter for 1064 nm and a horizontally (x) oriented polarization analyzer to block extraneous light from the PMT detector. In addition, all measurements were found to be independent of the pump beam polarization.

E. Excited-state DFWM dynamics

To study the dynamics of the excited-state DFWM, a transient pump-probe experiment is carried out by changing the path length of the pump beam while maintaining the DFWM probes. By observing the DFWM amplitude for many pump-probe delay times, we measure the time decay of the population responsible for the enhancement of the DPH susceptibility. The pump beam must be realigned for each delay position. This is accom-

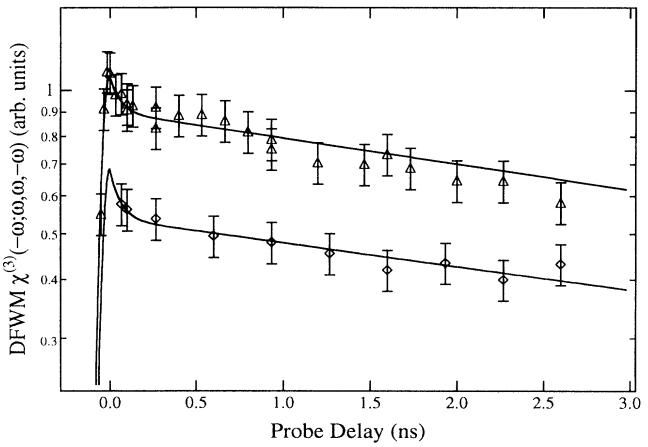

FIG. 7. The 1064-nm excited-state DFWM susceptibility is measured as a function of delay time between the 30-ps, 355-nm pump pulse and the two 30-ps, 1064-nm probe pulses. At zero delay, the signal is a maximum, and it decays (by nearly a single exponential with a decay time of 8ns ± 2ns for each of the 0.6 and 1.2 mM sample concentrations shown) with increasing pump-probe pulse delay time with respect to the pump pulse. Careful examination of the decay curves shows evidence for rapid 60-ps equilibration of the S_1 and S_2 excited states of DPH.

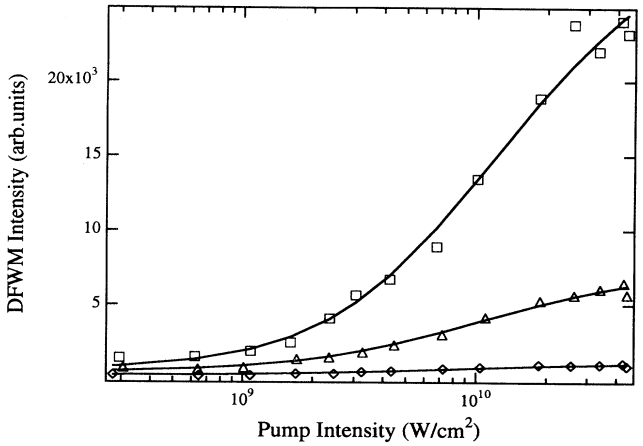

FIG. 8. The signal of the excited-state DFWM experiment is plotted as a function of the 355-nm pump intensity for several concentrations of DPH in dioxane. The saturation intensity is higher for higher concentrations, due to the more rapid decay observed for higher concentrations due to aggregation. All quantitative comparisons of $\chi^{(3)}$ for different concentrations is done using the maximum pump intensity, where the excited-state population is saturated for all concentrations: ◇, 1.6 mM; △, 3.3 mM; and □, 6.5 mM.

plished by computer control of the alignment optics that position the pump beam on the interaction region of the sample, and an algorithm that searches for the largest pump induced signal. The peak amplitude of such a scan was used for the signal amplitude at each delay. The data set can be fit to an exponential decay.

The technique involved in the study of the dynamics of the DFWM process is similar to the standard method of pump-probe absorption spectroscopy. In such an experiment, the transmission of a probe beam is monitored with respect to the arrival time of a pump beam. When the probe beam precedes the pump, it encounters only molecules in the ground state and, therefore, measures the DFWM susceptibility of the ground state. When the probe follows the pump, it encounters a mixture of molecules in the excited and ground states; and the DFWM signal is due to a susceptibility that is a sum of contributions from the solvent, excited-state molecules and ground-state molecules.

The excited-state population decays with increasing delay time, thus the DFWM signal also decays with an exponential time dependence,

$$\frac{I}{I_0} = e^{-\frac{2t}{\tau}}, \tag{3.12}$$

where the time constant is τ for the susceptibility and is $\tau/2$ for the signal amplitude. The excited-state lifetime of DPH in dilute solutions of dioxane measured by the excited state pump-probe DFWM experiment is 8 ns ± 2 ns shown for samples of 0.6 and 1.2 mM concentration in Fig. 7, in agreement with the lifetime determined by fluorescence decay studies of 7.8 ns [9]. The nonlinear optical enhancement we observe is, therefore, purely a result of the population of the electronic excited state of DPH.

F. Saturation of the pump effect

Since the excited-state DFWM signal depends on the population of the excited state, we expect the output intensity to saturate as a function of 355-nm pump intensity. Figure 8 shows the pump intensity data acquired for a range of sample concentrations in the pump-probe DFWM experiment, demonstrating the saturation effect. We fit each of the data sets to a function that incorporates the expression for the saturation of the excited-state population. With the pump on, the nonlinear susceptibility of the DPH sample is given by Eq. (3.8). The ground- and excited-state population densities are given in Eqs. (2.3) and (2.4), and can be used to arrive at the expression for $\chi^{(3)}$,

$$\chi^{(3)}(-\omega;\omega,\omega,-\omega) = (f_\omega)^4\left\{N_D\gamma^D(-\omega;\omega,\omega,-\omega) + c\frac{1}{2}\left[1+\frac{I_S}{I+I_S}\right]N_A\gamma^{S_0}(-\omega;\omega,\omega,-\omega)\right.$$
$$\left. + c\frac{1}{2}\left[1-\frac{I_S}{I+I_S}\right]N_A\gamma^{S_2}(-\omega;\omega,\omega,-\omega)\right\}. \tag{3.13}$$

TABLE I. The saturation intensities from excited-state DFWM measurements of DPH solutions are shown for several concentrations.

Concentration (mM)	I_S (W/cm^2)
1.6	5.8×10^9
3.3	6.2×10^9
6.5	6.5×10^9

If we make the assumption (valid for DPH) that $\gamma^{S_0} \ll \gamma^{S_2}$ and that N_D is constant for dilute solutions, we can simplify the above expression to obtain,

$$\chi^{(3)}(-\omega;\omega,\omega,-\omega) = \left\{K_1 + K_2\left[1 - \frac{I_S}{I+I_S}\right]\right\}, \quad (3.14)$$

where K_1 and K_2 are constants depending on the molecular susceptibilities of the dioxane and excited-state DPH, and on the concentration. For each sample concentration, the data are fit using Eq. (3.14), and the resulting values for I_S are given in Table I.

The important conclusion to derive from the dependence of the excited-state DFWM signal on pump intensity is that the saturation of the excited-state population in the simple two level model is sufficient to describe fully the saturation behavior of the experiment signal. We note that the saturation intensities observed are in agreement with separate single beam saturable absorption measurements described later.

In addition, for DFWM detected in the $2\mathbf{k}_2 - \mathbf{k}_1$ direction, the signal is proportional to the square of the intensity of probe two and proportional to the intensity of probe one. In the $2\mathbf{k}_1 - \mathbf{k}_2$ direction, the dependences are reversed. We observe the intensity dependences to be in agreement with the predicted behavior as shown in Fig. 9, where the DFWM signal is plotted with respect to each probe intensity and with respect to the total power in both probe beams.

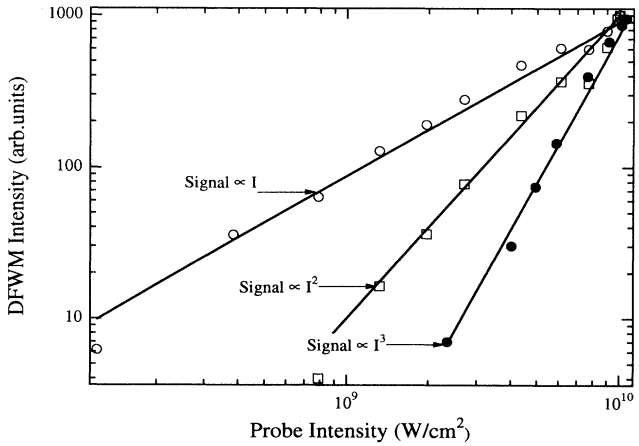

FIG. 9. The normalized excited-state DFWM signal is plotted as a function of probe intensity. The upper line shows the excited-state DFWM signal with respect to the intensity of the $\mathbf{k}_1$ probe. Since the excited state DFWM is in the $2\mathbf{k}_2 - \mathbf{k}_1$ direction, we compare to a line of slope 1 on this log-log plot. The middle line shows the signal with respect to the intensity of the $\mathbf{k}_2$ probe. We compare to a line of slope 2 since the signal depends on the square of the $\mathbf{k}_2$ intensity. The lower line shows the signal with respect to the overall 1064-nm probe power supplied to the experiment (before the probe beam splitter). We expect cubic dependence, and thus we compare with a line of slope 3. All the systematic probe power dependences agree with theoretical expectations within experimental uncertainty. The data in this figure have been arbitrarily normalized to the largest intensity. This way, the lines show the effect of attenuation of each of the probe beams from the maximum experiment signal.

IV. ADDITIONAL OPTICAL PROPERTIES OF DPH

A. Saturable absorption

Single beam saturable absorption measurements have been separately performed on solutions of DPH in dioxane. As the pump beam passes through a low (0.25 to 1 mM) concentration sample, the transmission is monitored as a function of intensity. We expect the transmission to saturate as a function of the incident intensity as the excited-state population attains its saturation value of $\rho_e = 1/2$. The transmission of the sample can be expressed as

$$\begin{aligned} T &= e^{-\alpha L}{}_e{}^{-\alpha_B L} \\ &= e^{-cN_A\sigma_g L(\rho_e - \rho_g)}{}_e{}^{-\alpha_B L} \\ &= e^{-cN_A\sigma_g L\frac{1}{1+\frac{I}{I_S}}}\, e^{-\alpha_B L}, \end{aligned} \quad (4.1)$$

where c is the concentration of the sample, L is the sample path length, σ_g is the ground-state absorption at 355 nm, I_S is the pump saturation intensity, α_B is any unsaturable background absorption due to excited-state absorption, and ρ_g and ρ_e are the two level model ground- and excited-state populations given in Eqs. (2.3) and (2.4). Typical values for these parameters are $L = 0.2$ mm, $c = 3$ mM, $-cN_A\sigma_g L = 3$, and $I_S = 2 \times 10^9$ $\frac{\text{W}}{\text{cm}^2}$.

The saturable absorption measurement is carried out by focusing a beam of 355-nm, 30-ps pulses into a flowing liquid sample cell containing the DPH solutions. Flowing the samples in the sample cell eliminates the thermal convection which would drive absorbing molecules away from the pumped region in a stationary liquid cell. The light that passes through the cell is collected by a lens and reflected into a (Hamamatsu model R/955) PMT. A wavelength filter in front of the PMT eliminates any other wavelength from contributing to the signal. A reference beam is split from the pump beam into another PMT (RCA model 31034), and the ratio of the signals from the two detectors, proportional to the transmission through the sample, is recorded for different intensities selected by the angle of the halfwave plate with respect to the angle of the polarizer in the pump beam.

Figure 10 shows the absorptivity observed for DPH samples of concentration 0.25 to 1 mM as a function of input intensity. A fit using the relation in Eq. (4.1) is used to calculate the saturation intensities presented in

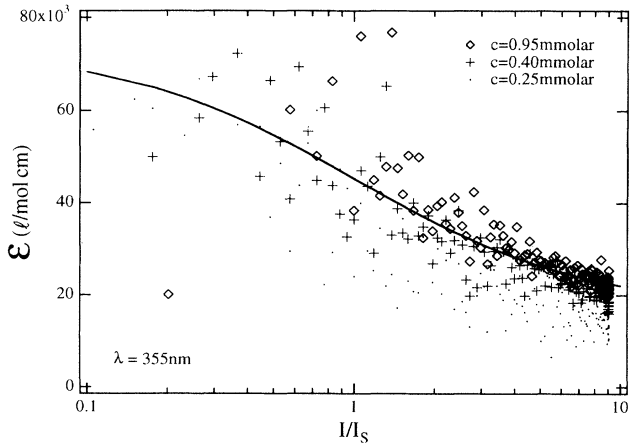

FIG. 10. The excited-state absorptivity ϵ is measured for several concentrations of DPH in dioxane, and the result is plotted as a function of pump intensity. ϵ is seen to saturate for all of the samples tested.

Table II. These values are comparable with the saturation intensities measured at different concentrations in the excited-state DFWM experiment.

B. Saturable absorption dynamics

Because of the nanosecond lifetime of DPH, the $S_0 \rightarrow S_2$ absorption is easily saturated by a 1-mJ, 30-ps, 355-nm laser pulse. This saturation is easily seen in the data of Kohler *et al.* [8], where the fluorescence of a free jet (gas phase) of DPH is observed to saturate as a function of the fluence of the exciting light. The transition can be described by a density matrix,

$$\rho = \begin{bmatrix} \rho_{gg} & \rho_{ge} \\ \rho_{eg} & \rho_{ee} \end{bmatrix}, \tag{4.2}$$

where ρ_{gg} is the population density of the S_0 ground state, and ρ_{ee} is the population of the S_2 excited state. When the absorption of such a two level system is saturated by a resonant optical pump and for times longer than the dephasing time T_2, the density matrix becomes,

TABLE II. The saturation intensities from saturable absorption measurements of DPH solutions are shown for several concentrations. Also shown are the unsaturable background absorptions, which are a measure of the excited-state absorption present at 355 nm from the excited state. The difference in the I_S values is the result, in part, of molecular aggregation at higher concentrations.

Concentration (mM)	I_S (W/cm^2)	αL_{bkg}
0.25	1.5×10^9	0.13
0.40	2.6×10^9	0.37
0.95	3.4×10^9	0.67

$$\rho = \begin{bmatrix} \frac{1}{2} & 0 \\ 0 & \frac{1}{2} \end{bmatrix}, \tag{4.3}$$

where half of the molecules in a sample are seen to occupy the excited state. After excitation to the excited state, ρ_{ee} decays exponentially with the aforementioned lifetime measured by excited-state absorption. Then,

$$\rho = \begin{bmatrix} \left(1 - \frac{1}{2}e^{-t/\tau}\right) & 0 \\ 0 & \frac{1}{2}e^{-t/\tau} \end{bmatrix} \tag{4.4}$$

describes the time evolution of the density matrix following excitation by a pump pulse with a pulse width much shorter than the excited-state lifetime τ.

Single frequency pump-probe transmission measurements are carried out using a weak 355-nm probe which follows a path equal in length to an intense 355-nm pump beam, which saturates the absorption of the probed region of the sample. A (Hamamatsu R/955) PMT detector with a preamplifier, detects the probe intensity. By changing the pump-probe delay time, we observe the transmission changes in the 355-nm probe, and observe the decay of the S_2 excited state with increasing probe delay. The transmission for a saturable absorber can be expressed as,

$$T = e^{cN_A\sigma_g L(\rho_g - \rho_e) - cN_A\sigma_e L\rho_e}, \tag{4.5}$$

and the data can be fit to an exponential decay using the relation,

$$\ln\left(\frac{\Delta T}{T} + 1\right) = cN_A\left(\sigma_g - \tfrac{1}{2}\sigma_e\right)Le^{-t/\tau} \tag{4.6}$$

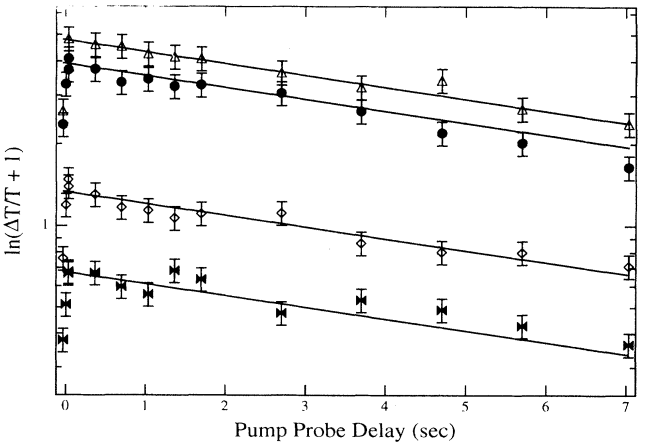

FIG. 11. The differential transmission of 30-ps, 355-nm pulses is observed as a function of pump-probe delay time for dilute solutions of DPH in dioxane. For each data point, we calculate the function $\ln\left(\frac{\Delta T}{T} + 1\right)$ which decays exponentially with the excited-state population. The curves correspond from bottom to top to concentrations of 0.31, 0.61, 1.13, and 1.47 mM, respectively, and the lifetime for all the samples is found to be (10.0 $\pm$ 2.5) ns.

with a lifetime corresponding to the relaxation from the initial S_2 population back to the ground state. In Fig. 11, the ground-state recovery time for samples of concentration 0.31 to 1.47 mM is seen to be 10.0 ± 2.5 ns, in agreement with the lifetime measured by excited-state pump-probe DFWM.

C. Excited-state absorption

Excited-state absorption (ESA) occurs when the excited state is the initial occupied state for a second one-photon absorbing electronic transition. Two ESA bands in DPH near 480 nm and 650 nm have been observed [21,10], corresponding to $S_1 \rightarrow S_n$ and $S_2 \rightarrow S_n$ transitions, respectively. After equilibration of the S_1 and S_2 state populations, the two ESA peaks decay simultaneously with the fluorescence decay lifetime. DPH shows no significant ESA above 800 nm [21].

We performed independent excited-state absorption tests at 1064 nm on DPH solutions excited by 30-ps pulses at 355 nm. Using a photodiode, we monitored the transmission of one of the 1064-nm probe beams from the DFWM apparatus through the DPH sample, and looked for any change in transmission caused by the presence of the pump. We found that there is no ESA at 1064 nm in DPH solutions within the experimental resolution. After observing the pump enhanced signal in the excited-state DFWM apparatus to verify that the beams are properly overlapped in the sample, a mirror was inserted behind the sample to reflect one 1064-nm probe onto a photodiode. Using this as a monitor of the transmission through the sample, no difference in the transmission in the presence or absence of the pump was observed. Thus, a limit for the magnitude of any change in transmission induced by the pump can be calculated from the fluctuations in the averaged differential transmission,

$$\frac{\Delta T}{T} = \frac{e^{-\alpha_e L} - e^{-\alpha_g L}}{e^{-\alpha_g L}} = e^{-(\alpha_e - \alpha_g) L} - 1. \quad (4.7)$$

At 1064 nm, $\alpha_g = 0$, and $\alpha_e = cN_A\rho_e\sigma_e$, where $\rho_e = 1/2$ in saturation. Then we have

$$\ln\left(\frac{\Delta T}{T} + 1\right) = -\tfrac{1}{2} cN_A\sigma_e L e^{-t/\tau}. \quad (4.8)$$

In the experiment, the differential transmission fluctuates about zero, and we arrive at the upper bound limit for the ESA,

$$\sigma_e(1064 \text{ nm}) < 2 \times 10^{-18} \text{ cm}^2 \quad (4.9)$$

The important conclusion, therefore, is that we observe no ESA at 1064 nm upon excitation by 355 nm in DPH.

V. CONCLUSION

The third-order optical susceptibility $\chi^{(3)}(-\omega_4;\omega_1,\omega_2,\omega_3)$ of organic and polymeric materials is being intensely investigated because nonresonant virtual excitation of the delocalized π-electron systems of these materials can result in large ultrafast nonlinear optical responses with minimal background absorption. We have demonstrated through experimental studies that $\chi^{(3)}(-\omega_4;\omega_1,\omega_2,\omega_3)$ can be increased by orders of magnitude over the normally observed ground-state values by population of electronic excited states. The excited-state enhancement mechanism was theoretically predicted by many-electron, configuration interaction calculations of the molecular susceptibility $\gamma_{ijkl}(-\omega_4;\omega_1,\omega_2,\omega_3)$ of one-dimensional chains when either the first or second π-electron excited state is occupied. The principal reasons for the enhancement are (1) larger optical transition moments $\mu_{nn'}$, (2) smaller transition energies between the occupied excited state S_n and other excited states $S_{n'}$, and (3) a reduced degree of competition between virtual excitation processes that has been shown to be a limiting factor in the ground state (S_0) $\gamma^{S_0}_{ijkl}(-\omega_4;\omega_1,\omega_2,\omega_3)$.

We have described recent excited-state DFWM measurements which show an increase as large as a factor of 100 in the completely nonresonant DFWM signal at 1064 nm when solutions of the conjugated linear chain DPH are optically pumped at 355 nm into the first optically allowed electronic excited state S_2. A large $\gamma^{S_2}(-\omega;\omega,\omega,-\omega)$ of $(12\,000 \pm 1700) \times 10^{-36}$ esu is observed compared to the ground state $\gamma^{S_0}(-\omega;\omega,\omega,-\omega)$ which is $< 50 \times 10^{-36}$ esu. Importantly, separate transient absorption experiments show there is no excited-state absorption at 1064 nm with excitation at 355 nm. Therefore, upon population of the excited state, the microscopic third-order optical susceptibility of DPH is increased by orders of magnitude without introducing any optical loss at the probe wavelength.

As is true of most DFWM experiments, we cannot entirely exclude the possibility of a molecular orientational contribution to the signal. However, electroabsorption measurements of a slightly longer, but otherwise identical, structure than DPH, diphenyloctatetraene, find an excited-state polarizability just slightly more than a factor of 3 larger than that of the ground state [29]. Since this is far short of the increase that would be required to account for the observed increase of the DFWM signal, and since the electronic contribution to $\chi^{(3)}(-\omega;\omega,\omega,-\omega)$ of the highly conjugated DPH structure is expected to be much larger than the orientational contribution, the orientational contribution is not expected to be significant in the observed enhancement.

The excited-state enhancement mechanism is generalizable to other nonlinear optical processes and to other material structures. The measurements reported to date were made in solutions where the small number density of excited-state molecules with large optical nonlinearity results in a smaller $\chi^{(3)}(-\omega_4;\omega_1,\omega_2,\omega_3)$ than would be observed with a pure, single substance. Studies are cur-

rently underway on pure polymer thin films where typical nonresonant ground-state $\chi^{(3)}$ values on the order of 10^{-11}–10^{-10} esu are expected to be enhanced by orders of magnitude, potentially leading to figures of merit sufficient for practical photonics devices.

ACKNOWLEDGMENTS

This work was generously supported by grants from AFOSR, DARPA, and the Pittsburgh Supercomputing Center.

* Present address: Department of Physics, Virginia Polytechnic Institute and State University, Blacksburg, Virginia 24061.

[1] L. R. Dalton, Nature **359**, 269 (1992).
[2] *Nonlinear Optical Properties of Organic and Polymeric Materials*, edited by D.J. Williams (American Chemical Society, Washington, D.C., 1983).
[3] *Nonlinear Optical Effects in Organic Polymers*, edited by J. Messier *et al.* (Kluwer Academic, Boston, 1989).
[4] *Organic Materials for Nonlinear Optics*, edited by R.A. Hann and D. Bloor (Royal Society of Chemistry, London, 1989).
[5] *Nonlinear Optical Properties of Materials*, edited by C.M. Bowden and J.W. Haus [J. Opt. Soc. Am. B **6**, 562 (1989)].
[6] Q.L. Zhou, J.R. Heflin, K.Y. Wong, O. Zamani-Khamiri, and A.F. Garito, Phys. Rev. A **43**, 1673 (1991); *Organic Molecules for Nonlinear Optics and Photonics*, Vol. 194 of *NATO Advanced Study Institute, Series E*, edited by F. Kajar and J. Messier (Kluwer Academic, Boston, 1991), pp. 239–262.
[7] J.R. Heflin, D.C. Rodenberger, R.F. Shi, M. Wu, N.Q. Wang, Y.M. Cai, and A.F. Garito, Phys. Rev. A **45**, R4233 (1992).
[8] B.E. Kohler and T.A. Spiglanin, J. Chem. Phys. **80**, 5465 (1984).
[9] E.D. Cehelnik, R.B. Cundall, J.R. Lockwood, and T.F. Palmer, J. Phys. Chem. **79**, 1369 (1975).
[10] C. Rulliere and A. Declemy, Chem. Phys. Lett. **135**, 213 (1987); P.C. Alford and T.F. Palmer, J. Chem. Soc. Faraday Trans. **79**, 433 (1983); Chem. Phys. Lett. **86**, 248 (1982).
[11] J.R. Heflin, K.Y. Wong, O. Zamani-Khamiri, and A.F. Garito, Phys. Rev. B **38**, 1573 (1988).
[12] J.W. Wu, J.R. Heflin, R.A. Norwood, K.Y. Wong, O. Zamani-Khamiri, and A.F. Garito, J. Opt. Soc. Am. B **6**, 707 (1989), and references therein.
[13] J.R. Heflin, Y.M. Cai, and A.F. Garito, J. Opt. Soc. Am. B **8**, 2132 (1991), and references therein.
[14] R.W. Boyd, *Nonlinear Optics* (Academic Press, New York, 1992).
[15] See, for example, A.E. Siegman, *Lasers* (University Science Books, Mills Valley, CA, 1986), pp. 204–206.
[16] D.C. Rodenberger, W. D. Chen, R. F. Shi, Q. L. Zhou, and A.F. Garito, Proc. SPIE **2025**, 56 (1993).
[17] See, for example, A. Kaltzbeitzel, D. Neher, C. Bubek, T. Sauer, B. Wegner, and W. Caseri, in *Electronic Properties of Conjugated Polymers*, edited by H. Kuzmany, M. Mehring, and S. Roth (Springer, New York, 1989); A. Kaltzbeitzel, Ph.D. dissertation, University of Mainz, 1989.
[18] T. Itoh and B.E. Kohler, J. Phys. Chem. **91**, 1760 (1987).
[19] B.E. Kohler and T.A. Spiglanin, J. Chem. Phys. **82**, 2939 (1985).
[20] B.S. Hudson, B.E. Kohler, and K. Schulten, in *Excited States*, edited by E.C. Lim (Academic Press, New York, 1982), Vol. 6.
[21] R.A. Goldbeck, A.J. Twarowski, E.L. Russel, J.K. Rice, R.R. Birge, E. Switkes, and D.S. Kliger, J. Chem. Phys. **77**, 3319 (1982).
[22] T. Kobayashi, A. Terasaki, T. Hattori, and K. Kurokawa, Appl. Phys. B **47**, 107 (1988).
[23] T. Hattori and T. Kobayashi, Chem. Phys. Lett. **133**, 230 (1987).
[24] C.V. Heer and N.C. Griffen, Opt. Lett. **4**, 239 (1979).
[25] A. Yariv and D.M. Pepper, Opt. Lett. **1**, 16 (1977).
[26] J. Etchepare, G.A. Kenney-Wallace, G. Grillon, A. Migus, and J.P. Chambaret, IEEE J. Quantum Electron. **QE-18**, 1826 (1982).
[27] D.C. Rodenberger, J.R. Heflin, and A.F. Garito, Nature **359**, 309 (1992).
[28] R.W. Hellwarth, Prog. Quantum Electron. **5**, 2 (1977).
[29] W. Liptay, R. Wortmann, H. Schaffrin, O. Burkhard, W. Reitinger, and N. Detzer, Chem. Phys. **120**, 439 (1988).